Singular Value Robustness Tests for Missile Autopilot Uncertainties

Kevin A. Wise*
McDonnell Douglas Missile Systems Company, St. Louis, Missouri 63166

Singular value robustness tests that evaluate missile autopilot sensitivity to neglected/mismodeled dynamics and real parameter variations are presented. Robustness theorems by Doyle and Lehtomaki are used to evaluate autopilot sensitivity to neglected and mismodeled actuator dynamics and neglected bending dynamics. The structured singular value μ-test of Doyle is used to compute a multivariable stability margin and to evaluate autopilot sensitivity to uncertain aerodynamic stability derivatives, modeled as real parameter variations. The conservatism of these robustness tests is discussed.

Introduction

MUCH recent attention has been focused on determining the robustness of multivariable feedback designs in the presence of uncertainties. In particular, this focus has been on frequency domain techniques (methods which employ singular value frequency responses). These new methods of analysis join, and in some cases replace, the classical Bode and Nyquist techniques with multivariable generalizations and extend many modeling uncertainty capabilities. This application paper presents a brief overview of the theory and methods available and demonstrates their application using a missile flight control system.

In the early 1980s, several papers appeared describing how multivariable feedback systems can be analyzed in the frequency domain.[1,2] The techniques introduced at that time use singular value matrix norms to analyze multi-input/multi-output (MIMO) feedback designs. One of the more noted applications of the singular value analysis technique was its application to linear quadratic (LQ) feedback designs. Anderson and Moore,[3] in an early text, described the stability characteristics of a single-input/single-output (SISO) LQ feedback design. It was shown that the Nyquist loci for an LQ state feedback design does not enter a unit disk centered at the $(-1, j0)$ point in the complex plane, guaranteeing a $(-1/2, +\infty)$ gain margin and a ± 60 deg phase margin. Using singular value matrix norms this same property was shown to hold for MIMO LQ state feedback designs.

Doyle[4] (and extensions made by Lehtomaki[5]) developed several robustness theorems, which were fundamental in developing the analysis techniques used to analyze model uncertainties. These methods utilize singular value theory as a means of measuring the size of MIMO frequency dependent matrices. The use of singular value theory has become very popular and several techniques have been developed for computing singular value gain and phase margins[6,7] with the creation of a universal gain and phase margin diagram.[7] This diagram and other methods as well were used to transform the singular value concepts into classical measures of stability and robustness with a focus on analyzing MIMO systems in the frequency domain. As a result of this work, significant insight was displayed[7] in relating the singular value gain and phase margin equivalents to their classical counterparts.

The singular value robustness tests developed by Doyle[4] and Lehtomaki[5] modeled control system uncertainties using a full single-block matrix structure. If the uncertainties were truly unstructured and in this form, then these tests are not conservative. If the uncertainties did enter the system in a structured way, these tests produced conservative estimates of stability robustness. This fact is demonstrated in this paper by comparing the stability robustness of two missile autopilot designs under structured and unstructured uncertainty.

Doyle[8,9] later developed a method of incorporating the structure of the uncertainty into the uncertainty analysis. This capability reduced the conservatism of the previous singular value techniques by utilizing a multiple-block diagonal structural model of the uncertainties. This test is called the structured singular value (SSV) μ-test.

One of the more important applications of the μ-test is the analysis of real parameter variations.[10] This particular type of problem has faced control system design engineers since the beginning. Classical gain and phase margins have been the answer to analyzing this problem in the past. Until recently, the classical linear analysis techniques were not useful in analyzing this problem, unless the problem was formulated into a root locus problem. When real parameter variations are modeled, they often appear nonlinearly in the characteristic equation. The methods developed by Morton[10,11] formulate the problem in such a manner that the μ-test, when applied, will conservatively analyze the real parameter variation.

In contrast to the above singular value based tests, robustness to uncertainties is also analyzed using polynomial methods. A myriad of papers which utilize Kharitonov's theorem[12] and variants thereof have recently been published. Kharitonov's theorem analyzes the robustness question by examining the Hurwitz (stability) properties of a family of polynomials whose coefficients are based upon the system's characteristic equation and uncertainties. Barmish[13] presents an excellent literature review on these polynomial methods.

Robustness Theory

Uncertainty models may be categorized as unstructured or structured. If the system's uncertainty is modeled as a full single-block matrix, the uncertainty is unstructured. If the uncertainty is modeled as a block diagonal matrix, the uncertainty is structured. Both unstructured and structured uncertainty analysis procedures use singular value theory to mea-

Received March 1, 1989; presented as Paper 89-3552 at the AIAA Guidance, Navigation, and Control Conference, Boston, MA, Aug. 14-16, 1989; revision received April 6, 1990.

*Staff Specialist, Advanced Guidance, Navigation, and Control; Dept. E431, Mail Code 3064045, P.O. Box 516.

sure the size of complex valued matrices. These methods are outlined in this section.

Unstructured Uncertainty Analysis

The robustness theorems which are used to analyze the uncertainty models are derived from an application of the multivariable Nyquist theorem (see Postlethwaite[14] or Athans[15] for a statement of the multivariable Nyquist theorem). Consider the system shown in Fig. 1. The basic problem is to determine the robustness of the design in the presence of uncertainties. This design has the state space realization using the triple (A,B,K) with the loop transfer matrix (LTM) given by

$$L(s) = K(sI - A)^{-1}B \tag{1}$$

We wish to determine to what extent the parameters in the LTM can vary without compromising the stability of the closed-loop system. It can be shown[14] that

$$\det[I + L(s)] = \phi_{cl}(s)/\phi_{ol}(s) \tag{2}$$

where

$\phi_{ol}(s) = \det[sI - A]$: open-loop characteristic polynomial

$\phi_{cl}(s) = \det[sI - A + BK]$: closed-loop characteristic polynomial

Let $N(b_1, f(s), D)$ denote the number of encirclements of the point b_1 by the locus of $f(s)$ as s transverses the closed contour D in the complex plane in a clockwise sense. Using these definitions the multivariable Nyquist theorem can be stated in the following form.

Theorem 1: Multivariable Nyquist Theorem[15]

The system of Fig. 1 will be closed-loop stable in the sense that $\phi_{cl}(s)$ has no closed right half plane zeros if and only if for all R sufficiently large

$$N(0, \det[I + L(s)], D_R) = -P \tag{3}$$

or equivalently

$$N(-1, -1 + \det[I + L(s)], D_R) = -P \tag{4}$$

where D_R is the standard Nyquist D contour, which encloses all P closed right half plane zeros of $\phi_{ol}(s)$. Note that $N(b_1, f(s), D)$ is indeterminate if $\phi(s_0) = b_1$ for some s_0 on the contour D.

The stability robustness of a multivariable system can be observed by the near singularity of its return difference matrix (RDM) $I + L(s)$ at some frequency $s = j\omega_0$. If $I + L(s)$ is nearly singular, then a small change in $L(s)$ could make $I + L(s)$ singular. From a SISO viewpoint, this is the distance from the $(-1, j0)$ point in the complex plane made by the gain loci $L(j\omega)$. If the gain loci then encircle the $(-1, j0)$ point, instability results. The robustness theory discussed here gives an analogous distance measure for multivariable systems.

The multivariable Nyquist theorem is of little applicability as a robustness indicator because the $\det[I + L(s)]$ does not indicate the near singularity of $I + L(s)$. The multivariable Nyquist theorem only determines absolute stability. To determine the degree of robustness for a multivariable system, the singular value matrix norm is used. This matrix norm will determine the near singularity of the RDM.

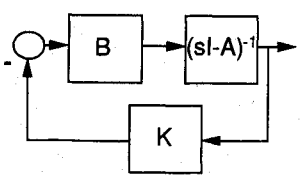

Fig. 1 State feedback control system.

Examining the magnitude of the singular values of the return difference matrix will indicate how close the matrix is to being singular. This measure of closeness to singularity is used in forming a multivariable gain margin, similar to the classical gain margin. However, as with many matrix norms, there is a restriction on the applicability of the singular value analysis. This restriction states that the compensated system described using the LTM $L(s)$ is closed-loop stable.

The singular value decomposition (SVD)[16] of the complex $n \times m$ matrix A is $A = U\Sigma V^*$, where U and V are unitary matrices, whose columns denote left and right singular vectors of the matrix A. The nonzero portion of the singular value matrix is

$$\Sigma = \text{diag}[\sigma_1 \cdots \sigma_k] \tag{5}$$

The singular values are ordered in size with $\bar{\sigma} = \sigma_1$ the largest and $\underline{\sigma} = \sigma_k$ the smallest (if A is a square singular matrix, then $\underline{\sigma} = 0$).

Classical gain and phase margins are used to measure the robustness of SISO systems to perturbations in the feedback loop. Singular values are used in measuring the robustness of multivariable systems. Let $L'(s)$ denote the perturbed LTM, which represents the actual system and differs from the nominal LTM $L(s)$ because of uncertainties in the open-loop plant model. Assume that $L'(s)$ has the state space realization (A', B', K') and open- and closed-loop polynomials given by

$$\phi'_{ol}(s) = \det[sI - A'] \tag{6a}$$

$$\phi'_{cl}(s) = \det[sI - A' + B'K'] \tag{6b}$$

respectively. Define $L(s,\epsilon)$ as a matrix of rational transfer functions with real coefficients which are continuous in ϵ for all ϵ such that $0 \le \epsilon \le 1$ and for all $s \in D_R$, which satisfies $L(s,0) = L(s)$ and $L(s,1) = L'(s)$. Using these definitions of the perturbed model, we are ready to state the fundamental robustness theorem of Lehtomaki.

Theorem 2: Fundamental Robustness Theorem[5]

The polynomial $\phi'_{cl}(s)$ has no closed right half plane zeros, and the perturbed feedback system is stable if the following holds:

1) $\phi_{ol}(s)$ and $\phi'_{ol}(s)$ have the same number of closed right half plane zeros; $\phi_{cl}(s)$ has no closed right half plane zeros.

2) $\det[I + L(s,\epsilon)] = 0 \ \forall \ (s,\epsilon)$ in $D_R \times [0,1]$ and $\forall \ R$ sufficiently large.

This theorem states that the closed-loop perturbed system will be stable, if by continuously deforming the Nyquist loci for the nominal $L(s)$ into that of the perturbed system $I + L(s,\epsilon)$, the number of encirclements of the critical point is the same for $L'(s)$ and $L(s)$, then no closed right half plane zeros were introduced into $\phi'_{cl}(s)$, resulting in a stable closed-loop system.

This theorem is used to develop simple tests for different types of model error characterizations. Just as there is not a unique representation for dynamic systems, there are many different forms for describing their modeling errors. The most common model error characterizations are additive errors and multiplicative errors (also described as relative or absolute errors). The classical gain and phase margins are associated with multiplicative error models since these margins are multiplicative in nature. (See Doyle,[9] Table 1, for representative types of uncertainty characterizations.)

Let $E(s)$ denote the modeling error under consideration. The additive model error is given by

$$E_a(s) = L'(s) - L(s) \tag{7}$$

and the multiplicative model error is given by

$$E_m(s) = [L'(s) - L(s)]L^{-1}(s) \tag{8}$$

The perturbed LTM can be constructed using Eqs. (7) and (8). For the additive error model, we have

$$L(s,\epsilon) = L(s) + \epsilon E_a(s) \tag{9}$$

and for the multiplicative error model we have

$$L(s,\epsilon) = [I + \epsilon E_m(s)]L(s) \tag{10}$$

Both Eqs. (7) and (8) imply the same $L(s,\epsilon)$ using different model error characterizations. In both Eqs. (7) and (8), $L(s,\epsilon)$ is given by

$$L(s,\epsilon) = (1-\epsilon)L(s) + \epsilon L'(s) \tag{11}$$

showing that $L(s,\epsilon)$ is continuous in ϵ for $\epsilon \in [0,1]$ and for all $s \in D_R$.

We have now defined the true perturbed plant model in terms of its nominal design model and the uncertainty matrix. The fundamental robustness theorem uses the return difference matrix $I + L(s, \epsilon)$ to determine if the number of encirclements of the critical point will change with the uncertainties. This happens when $I + L(s,\epsilon)$ becomes singular, in which case the $\det[I + L(s,\epsilon)] = 0$.

Using the multiplicative error characterization, the RDM is

$$I + L(s,\epsilon) = I + L(s) + E_m(s)L(s) \tag{12}$$

or

$$I + L(s,\epsilon) = A + B$$

with $A = I + L(s)$ and $B = E_m(s)L(s)$. For the perturbed system to be unstable, viewed through a change in the number of encirclements of the $\det[I + L(s,\epsilon)]$, the matrix $A + B$ must be singular for some $\epsilon \in [0,1]$ and $s \in D_R$. We know that A is nonsingular (the RDM of the nominal design) since the nominal design is closed-loop stable. Thus, if the uncertainty is going to create instability, then the matrix B, when added to A, must make $A + B$ singular.

The use of singular values plays an important role in analyzing the near singularity of matrices. The maximum and minimum singular values of the matrix A are defined as

$$\bar{\sigma}[A] = \max_{x \neq 0} \frac{||Ax||_2}{||x||_2} = ||Ax||_2 \tag{13a}$$

$$\underline{\sigma}[A] = \min_{x \neq 0} \frac{||Ax||_2}{||x||_2} \tag{13b}$$

The minimum singular value $\underline{\sigma}[A]$ measures the near singularity of the matrix A. Assume that the matrix $A + B$ is singular. If $A + B$ is singular then $A + B$ is rank deficient. Since $A + B$ is rank deficient, then there exists a vector $x \neq 0$ with unit magnitude ($||x||_2 = 1$) such that $(A + B)x = 0$ (x is in the null space of $A + B$). This leads to $Ax = -Bx$ with $||Ax||_2 = ||Bx||_2$. Using the above singular value definitions and $||x||_2 = 1$, we obtain the following inequality.

$$\underline{\sigma}[A] \leq ||Ax||_2 = ||Bx||_2 \leq ||B||_2 = \bar{\sigma}[B] \tag{14}$$

To be singular, $\underline{\sigma}[A] \leq \bar{\sigma}[B]$. To be nonsingular, $\underline{\sigma}[A] > \bar{\sigma}[B]$. This is precisely how the stability robustness tests are derived.

Theorem 3: Stability Robustness Theorem – Additive Uncertainty Model

The polynomial $\phi'_{cl}(s)$ has no closed right half plane zeros and the perturbed feedback system is stable if the following holds:

1) $\phi_{cl}(s)$ has no closed right half plane zeros.
2) $\underline{\sigma}[I + L(s)] \geq \bar{\sigma}[E_a(s)]$ $\forall$ $s \in D_R$ and for all R sufficiently large, with $E_a(s)$ given by Eq. (7).

See Lehtomaki[5] for proof of this theorem.

Theorem 4: Stability Robustness Theorem – Multiplicative Uncertainty Model

The polynomial $\phi'_{cl}(s)$ has no closed right half plane zeros, and the perturbed feedback system is stable if the following holds:

1) $\phi_{cl}(s)$ has no closed right half plane zeros.
2) $\underline{\sigma}[I + L^{-1}(s)] > \bar{\sigma}[E_m(s)]$ $\forall$ $s \in D_R$ and for all R sufficiently large, with $E_m(s)$ given by Eq. (8).

The proof of this theorem uses the singularity of $A + B$ argument. Stability of the perturbed closed-loop system is guaranteed for a nonsingular $I + L(s,\epsilon)$. Thus,

$$I + L(s,\epsilon) = L(s)[I + L^{-1}(s) + \epsilon E_m(s)] \tag{15}$$

Here we assume that $L^{-1}(s)$ exists. If $I + L(s,\epsilon)$ is to be singular, then $[I + L^{-1}(s) + \epsilon E_m(s)]$ must be singular. Thus, to be nonsingular

$$\underline{\sigma}[I + L^{-1}(s)] > \bar{\sigma}[\epsilon E_m(s)] \tag{16}$$

or

$$\underline{\sigma}[I + L^{-1}(s)] > \epsilon\bar{\sigma}[E_m(s)] \tag{17}$$

$$\underline{\sigma}[I + L^{-1}(s)] > \bar{\sigma}[E_m(s)] \tag{18}$$

Depending upon the model error characterization, either additive or multiplicative, the robustness test is different. Theorems 3 and 4 are sufficient tests for stability. As long as the singular value frequency responses do not overlap, stability is guaranteed.

Structured Uncertainty Analysis: Complex Variations

The SSV analysis was developed by Doyle[9] to reduce the conservatism of evaluating stability robustness using unstructured singular value computations. By structuring the uncertainty model into a block diagonal matrix form, and applying the SSV μ-test, a less conservative estimate of stability robustness is obtained. See Doyle[9] for details on the derivation of the SSV μ.

The modeling error matrix $E(s)$, Eqs. (7) and (8), assumes that the matrix is full and arbitrary in form. The SSV approach better defines the allowable uncertainties, which structures the matrix $E(s)$. A better known uncertainty model will yield a less conservative analysis of the stability robustness. The first step in the SSV analysis is to define the block diagonal perturbation (BDP) problem.

For the BDP problem, we want to transform the general feedback system of Fig. 2a into the BDP structure of Fig. 2b. The matrix $\Delta(s)$ describes the allowable uncertainties (possibly complex) in the system.

The matrix $\Delta(s)$ is a block diagonal matrix, with each matrix entry $\Delta_i(s)$ on the diagonal corresponding to a matrix of perturbations occurring in the system. The matrix $-M(s)$ is the transfer function between the output of the perturbation to its input. The matrix depends upon $K(s)$, $G(s)$, and the structure of the perturbations. $M(s)$ is a block matrix where

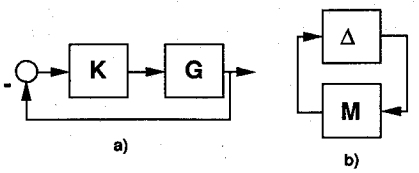

Fig. 2 Block diagonal structure.

the i,jth block $M_{ij}(s)$ is the negative of the transfer function from the output of $\Delta_j(s)$ to the input of $\Delta_i(s)$.

For example, consider the system in Fig. 3. For simultaneous input and output perturbations (Δ_1, and Δ_2 both arbitrary), we have

$$M = \begin{bmatrix} (I+KG)^{-1}KG & (I+KG)^{-1}K \\ -(I+GK)^{-1}G & -(I+GK)^{-1}GK \end{bmatrix};$$

$$\Delta = \begin{bmatrix} \Delta_1 & 0 \\ 0 & \Delta_2 \end{bmatrix} \tag{19}$$

In order for the BDP structure to ensure stability for the perturbed system, the nominal design without perturbation must be closed-loop stable. Considering the input and output perturbations described in Fig. 3, stability for the perturbed system is guaranteed only when

$$\det[I + K(I+\Delta_2)G(I+\Delta_1)] \neq 0, \forall \Delta_1, \Delta_2 \text{ and } \forall s \in D_R \tag{20}$$

Using the BDP structure, this is equivalent to

$$\det[I + M\Delta] \neq 0, \forall \Delta = \text{diag}(\Delta_1, \Delta_2) \text{ and } \forall s \in D_R \tag{21}$$

The object of the SSV analysis is to bound the size of Δ, viewed through a matrix norm, such that Eq. (21) is satisfied.

We can intuitively define the bound on the norm of Δ by using the $A + B$ argument of the preceding section. If $\det[I + M\Delta] = 0$, then from the $A + B$ argument, we know that

$$\underline{\sigma}[I] > \bar{\sigma}[M\Delta] \tag{22}$$

Using $\bar{\sigma}[M\Delta] < \bar{\sigma}[M]\bar{\sigma}[\Delta]$, and the fact that $\underline{\sigma}[I] = 1$, we obtain what is referred to as the small gain theorem

$$\bar{\sigma}[\Delta] < 1/\bar{\sigma}[M] \tag{23}$$

The small gain theorem (SGT) is a sufficient test for stability. If it is violated, the system may still be stable. In order to bound the magnitude of the real parameter variations modeled in Δ, we use the minimum of the $1/\bar{\sigma}[M]$ frequency response and use this bound at all frequencies. The conservatism in this bound is due to the 2-norm measure $\|M\|_2$. This bound on Δ assumes that Δ is a full matrix, when in fact it is diagonal. This is a conservative bound on Δ produced by the SGT.

The SSV μ analysis utilizes a block diagonal structure for Δ in Eq. (23) to develop a less conservative analysis. For a formal definition of μ, see Doyle.[9] Using this restriction for Δ, the size of Δ is limited through the restriction:

$$\bar{\sigma}[\Delta] < 1/\mu \tag{24}$$

The problem is to find the smallest μ such that for a block diagonal Δ the system remains stable. The SGT would ignore the structure of Δ and would result in $\mu = \bar{\sigma}[M]$, which is a worst case scenario (this would assume Δ to be a full single-block matrix, which would be conservative if Δ was actually block diagonal). Since the off diagonal terms in Δ are restricted to be zero by the block diagonal restriction, $\mu \leq \bar{\sigma}[M]$ with a strong inequality for diagonal Δ. A detailed derivation of the SSV μ can be found in Doyle.[9] The SSV μ is computed by bounding μ through the following optimization

$$\max_W |\lambda_{\max}(WM)| < \mu < \inf_D \bar{\sigma}[DMD]^{-1} \tag{25}$$

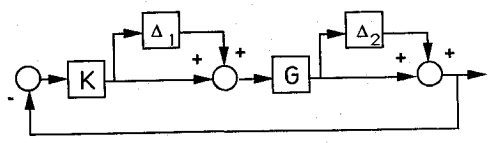

Fig. 3 Control system model with input/output uncertainties.

The analysis software used in this paper computes only the upper bound on μ by using the D-matrix optimization. Since the matrix M is frequency dependent, the D-matrix optimization is swept over a frequency range. This produces an upper bound on μ, which is frequency dependent. The minimum of the $1/\mu$ frequency response is used to bound $\bar{\sigma}[\Delta]$. The lower bound on μ provides directional information on the destabilizing perturbations. This would indicate which perturbation causes the system to be unstable. If both the upper and lower bound were computed, the amount of conservatism in μ would be evident by the spread between the upper and lower bounds.

Autopilot and Missile Airframe Dynamics

In this section, finite-dimensional linear time invariant models are presented which are used to design the autopilots. The dynamics of the missile have been separated into decoupled linearized pitch and roll-yaw subsystems. The pitch autopilot commands normal body acceleration. The roll-yaw autopilot commands a stability axis roll rate (roll rate about the velocity vector).

The conventional longitudinal flight control system for a missile airframe is shown in Fig. 4. Using block diagram manipulations, the block diagram of Fig. 4 is transformed into the block diagram of Fig. 2a. In Fig. 2a the transfer function matrix $K(s)$ describes only controller dynamics. The nominal rigid body longitudinal dynamics, containing uncertain parameters, is represented by $G(s)$.

The states modeled in the open-loop rigid body airframe model are angle of attack α (rad) and pitch rate q (rad/s). The output variables are acceleration A_z (ft/s^2) and pitch rate q. The state equations are

$$\dot{\alpha} = Z_\alpha \alpha + Z_\delta \delta + q \tag{26a}$$

$$\dot{q} = M_\alpha \alpha + M_\delta \delta \tag{26b}$$

with $A_z = VZ_\alpha \alpha + VZ_\delta \delta$.

The aerodynamics are modeled at Mach 0.8 ($V = 886.78$ ft/s) and an altitude of 4000 ft. At a trim angle of attack of 6 deg, the linearized airframe is open-loop stable in pitch. At a trim angle of attack of 16 deg, the airframe is open-loop unstable. Table 1 displays the nominal aerodynamic stability derivatives (Z_α, Z_δ, M_α, M_δ) at both of these conditions. The autopilot design $K(s)$ stabilizes the nominal plant model $G(s)$ using output feedback, as shown in Fig. 4, and provides acceleration command following.

The body axis roll-yaw flight control design equations are

$$\dot{\beta} = p\sin(\alpha) - r\cos(\alpha) + Y_\beta \beta + Y_{\delta a}\delta_a + Y_{\delta r}\delta_r \tag{27a}$$

$$\dot{r} = N_\beta \beta + N_{\delta a}\delta_a + N_{\delta r}\delta_r \tag{27b}$$

$$\dot{p} = L_\beta \beta + L_{\delta a}\delta_a + L_{\delta r}\delta_r \tag{27c}$$

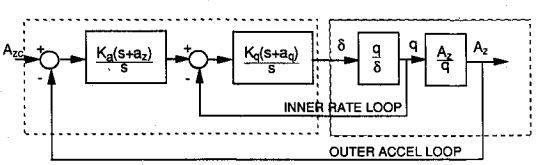

Fig. 4 Longitudinal autopilot.

Table 1 Nominal Aerostability Derivatives

	Pitch			
α,deg	Z_α,1/s	Z_δ,1/s	M_α,1/s^2	M_δ,1/s^2
6	−0.8757	−0.1531	−68.0209	−74.9210
16	−1.2100	−0.1987	44.2506	−97.2313
	Roll-yaw			
α,deg	Y_β,1/s	$Y_{\delta a}$,1/s	$Y_{\delta r}$,1/s	
6	−0.0251	0.1228	−0.2763	
16	−0.0052	0.1338	−0.1004	
	L_β,1/s^2	$L_{\delta a}$,1/s^2	$L_{\delta r}$,1/s^2	
6	574.7	195.5	−529.4	
16	556.8	70.2	−1879.0	
	N_β,1/s^2	$N_{\delta a}$,1/s^2	$N_{\delta r}$,1/s^2	
6	16.20	−53.61	33.250	
16	5.679	−57.03	5.7471	

where β is sideslip angle (rad), p is body roll rate (rad/s), r is body yaw rate (rad/s), and δ_a and δ_r are aileron and rudder fin deflections (radians). The variables Y_β, $Y_{\delta a}$, $Y_{\delta r}$, L_β, $L_{\delta a}$, $L_{\delta r}$, N_β, $N_{\delta a}$, and $N_{\delta r}$ are dimensional aerodynamic stability derivatives obtained from aerodynamic measurements of lateral side force and roll and yaw moments. Nominal values for these variables are listed in Table 1.

The stability axis coordinate system is defined as the transformation of body axes to the stability axes using angle of attack α. Wind axis coordinate system is defined as the transformation of stability axes to wind axes using sideslip angle β. The missile velocity vector is pointed along the x-axis of the wind coordinate system. In a bank-to-turn (BTT) autopilot, induced roll is minimized by rolling the missile about the velocity vector. Assuming that β is very small, this is a rotation about the x-axis in the stability axis coordinate system.

The roll-yaw autopilot taken from Wise[17] transforms the body axis dynamics to stability axes and uses plant shaping gains to decouple roll and yaw input channels. The rate loops are then closed using proportional-plus-integral control elements.

Autopilot Uncertainty Analysis in the Frequency Domain

In this section robustness theory is applied to the uncertainties created by mismodeled and/or neglected actuator dynamics, neglected bending dynamics, and aerodynamic uncertainties modeled as real parameter variations. These uncertainties are modeled and analyzed using unstructured and structured singular value-based robustness tests.

Actuator Uncertainty Analysis

Here we demonstrate the application of the stability robustness theorem in determining autopilot sensitivity to knowledge of the actuator dynamics. We examine two cases: 1) neglected actuator dynamics and 2) mismodeled actuator dynamics. An open-loop stable flight condition is used (trim angle of attack of 6 deg).

Missile autopilots are designed before many of the subsystem component specifications, such as those for actuators, have been defined. The following analysis shows how to evaluate autopilot sensitivity to control actuation system specifications using singular value robustness theory.

Neglected Actuator Dynamics

Figure 2a displays the autopilot transfer function $K(s)$ and uncertain missile dynamics $G(s)$. For a multiplicative uncertainty at the plant input, we have

$$G(s) = G_0(s)[1 + E_m(s)] \tag{28}$$

The nominal pitch open-loop transfer matrix is $G_0(s)$, with elevon fin deflection δ as the input and normal body acceleration A_z and pitch rate q as the outputs. The autopilot gains in Fig. 4 are $K_a = -0.001$, $a_z = 3.0$, $K_q = -0.2$, and $a_q = 3.0$. The scalar pitch loop transfer function $L(s)$, at the plant input, for the true model is

$$L'(s) = K(s)G_0(s)[1 + E_m(s)] \tag{29}$$

For the nominal design model,

$$L(s) = K(s)G_0(s) \tag{30}$$

Using a second-order transfer function model for actuator dynamics, the multiplicative uncertainty model $E_m(s)$ created by neglecting the dynamics is given by

$$E_m(s) = \frac{\delta(s)}{\delta_c(s)} - 1 = \frac{-s(s + 2\zeta\omega_a)}{s^2 + 2\zeta\omega_a s + \omega_a^2} \tag{31}$$

where $\zeta = 0.6$ and ω_a is treated as the unknown actuator natural frequency.

The roll-yaw open-loop transfer matrix is a 3 × 2 matrix, with aileron δ_a and rudder δ_r fin deflections as control inputs and lateral acceleration A_y, roll rate p, and yaw rate r as outputs. The compensator matrix $K(s)$ containing plant shaping gains and conventional proportional-plus-integral control elements, taken from Wise,[17] is

$$K(s) = \begin{bmatrix} K_1 & K_2 \\ K_3 & K_4 \end{bmatrix} \begin{bmatrix} 0 & K_p(s + a_p)/s & 0 \\ 0 & 0 & K_r \end{bmatrix} \tag{32}$$

where $K_p = 0.0135$, $a_p = 4.0$, $K_r = -0.173$, $K_1 = 1.0143$, $K_2 = -0.1472$, $K_3 = -0.4691$, and $K_4 = 0.6789$. The multiplicative uncertainty model describing neglected actuator dynamics is a 2 × 2 matrix with Eq. (31) on the diagonal elements.

Our goal is to show that the pitch and roll-yaw designs are robust to neglected actuator dynamics. To show this we apply the stability robustness theorem 4 and establish that

$$\underline{\sigma}[I + L^{-1}(s)] > \bar{\sigma}[E_m(s)] \forall s \in D_R \tag{33}$$

with $L(s)$ given by Eq. (30).

The above singular value frequency response comparison is only a sufficient test for stability. As long as the singular value frequency responses do not overlap, stability is guaranteed. This robustness test is used here to determine the lowest actuator natural frequency (actuator dynamics) that guarantees stability. After a missile autopilot has been designed to meet performance goals, this test can be used to define minimum control actuation system specifications.

Figure 5 displays the stability robustness theorem applied to the pitch and roll-yaw flight control systems. The intersection

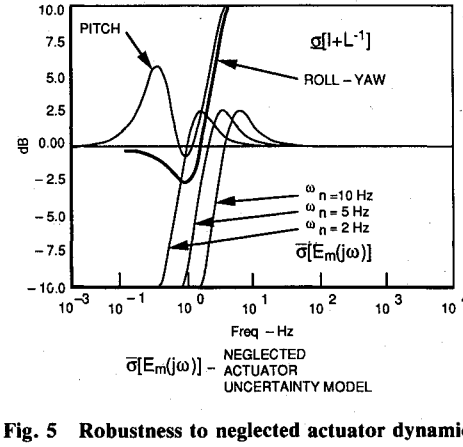

Fig. 5 Robustness to neglected actuator dynamics.

of $\underline{\sigma}[I + L^{-1}(s)]$ and $\bar{\sigma}[E_m(s)]$ violates the stability robustness theorem, which indicates that the closed-loop system is not guaranteed to be unstable. (An eigenanalysis performed on both the pitch and roll-yaw systems did show unstable closed-loop systems.) It should be evident from these two figures that the dip below 0 dB made by the $\underline{\sigma}[I + L^{-1}(s)]$ frequency locus, as well as the frequency at which the dip occurs, plays an important role in creating a robust design. Figure 5 shows both pitch and roll-yaw flight control designs to be equally sensitive to neglected actuator dynamics. This was expected since both designs were designed to have similar stability margins. In pitch, Eq. (33) is violated for $\omega_a < 2.8$ Hz. In roll-yaw, Eq. (33) is violated for $\omega_a < 2.1$ Hz. These results show that stability for the missile flight control system is not guaranteed for actuator natural frequencies below 2 Hz. Performing this analysis at the highest dynamic pressure flight condition (this is where the flight control system usually has the highest bandwidth) would indicate the minimum actuator natural frequency required to guarantee stability.

Mismodeled Actuator Dynamics

In this case the actuator dynamics are included in the design, but the natural frequency is mismodeled using the relation $\omega_{\text{true}} = \epsilon\omega_a$. The nominal actuator natural frequency is assumed to be 10.8 Hz. The multiplicative uncertainty model for this case is

$$E_m(s) = \frac{-s[(1-\epsilon^2)s + 2\zeta\omega_a\epsilon(1-\epsilon)]}{s^2 + 2\zeta\omega_a\epsilon s + \omega_a^2\epsilon^2} \tag{34}$$

Figure 6 displays the results of the stability robustness theorem applied to the pitch and roll-yaw flight control designs (created using the nominal actuator model) using a mismodeled actuator multiplicative uncertainty model. Figure 6 shows that when the true actuator natural frequency approaches 2 Hz, Eq. (33) is violated. Even though the design model included a nominal actuator model, we chose (for illustrative purposes only) to use the same autopilot gains. Thus, the mismodeled actuator uncertainty analysis predicts the same actuator natural frequency as the neglected actuator uncertainty analysis.

We have demonstrated using the singular value-based stability robustness theorem a method which predicts autopilot sensitivity to uncertain actuator design parameters. This analysis indicates the minimum actuator natural frequency which guarantees stability and the sensitivity to knowing this frequency.

Bending Uncertainty Analysis

The effectiveness of bending compensation can be evaluated by modeling neglected bending dynamics as a multiplicative plant input uncertainty and by applying Eq. (33). Both pitch and roll-yaw autopilot designs were designed ignoring flexible body dynamics. In the pitch flight control design, a notch filter centered at the first pitch bending mode (35.2 Hz) combined with a 30 Hz low pass filter is used to compensate for bending. In the roll-yaw design, a notch filter at 49.3 Hz is used with a 30 Hz low pass filter. The stability robustness theorem is used to show that the closed-loop system will be stable using bending compensation inserted into the feedback path. We present only the roll-yaw results.

Figure 7 displays the roll-yaw loop $\underline{\sigma}[I + L^{-1}(s)]$ vs frequency using flight control designs with and without bending compensation, and compares $\underline{\sigma}[I + L^{-1}(s)]$ with $\bar{\sigma}[E_m(s)]$. The multiplicative uncertainty model $E_m(s)$ results from neglecting the first two roll-yaw bending modes. The dashed curve in Fig. 7 is $\underline{\sigma}[I + L^{-1}(s)]$ with no bending compensation. The figure shows that $\underline{\sigma}[I + L^{-1}(s)]$ and $\bar{\sigma}[E_m(s)]$ overlap. A closed-loop eigenanalysis indicates that the roll-yaw system including bending is in fact closed-loop unstable. Figure 7 shows that the $\underline{\sigma}[I + L^{-1}(s)]$ locus using bending compensation does not intersect $\sigma[E_m(s)]$. Thus, the added bending compensation stabilizes the flexible system.

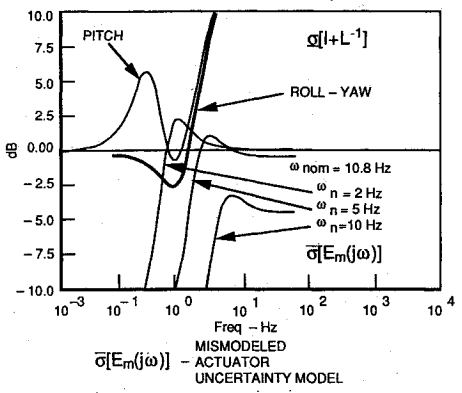

Fig. 6 Robustness to mismodeled actuator dynamics.

Application of the μ-test: Multivariable Stability Margin

This section compares the stability robustness of two roll-yaw bank-to-turn autopilot designs.[17,18] In addition to comparing these autopilots, the conservatism that results from modeling the uncertainties as a full single-block matrix vs a multiple-block diagonal matrix is demonstrated.

The SSV analysis was developed by Doyle[9] to reduce the conservatism of evaluating stability robustness using singular value techniques. The SSV approach better defines the allowable uncertainties, structuring the matrix $E_m(s)$. By structuring the allowable perturbations, less conservative estimates of stability robustness are produced. Here we will change the previous notation and denote uncertainties $E_m(s)$ as perturbations $\Delta(s)$.

The stability robustness of two autopilot designs are compared by applying the SSV μ-test and varying the structure of the allowable perturbations. The first autopilot design is a lateral-directional stability axis roll-rate command autopilot, denoted as plant shaping pole placement[17] (PSPP), Eq. (32). The second design is a linear quadratic Gaussian with loop transfer recovery (LQG/LTR) design which incorporates integral control [robust servo (RS)] in commanding a stability axis roll-rate. The RS LQG/LTR design is from Wise.[18] The open-loop roll-yaw plant $G_0(s)$ has two inputs and three outputs. The frequency dependent LTM $L(s)$, examined at the plant input, is of dimension 2×2 and always has full rank. The LTM L (s), examined at the plant output, is of dimension 3×3.

Using plant input and output multiplicative uncertainty (perturbation) models, we have

Input perturbation

$$G(s) = G_0(s)[I_2 + \Delta_1(s)]$$

Output perturbation

$$G(s) = [I_3 + \Delta_2(s)]G_0(s)$$

Simultaneous input-output perturbations

$$G(s) = [I_3 + \Delta_2(s)]G_0(s)[I_2 + \Delta_1(s)]$$

When we form the general BDP problem for these perturbations, we have

$$M = \begin{bmatrix} (I + KG)^{-1}KG & (I + KG)^{-1}K \\ -(I + GK)^{-1}G & (I + GK)^{-1}GK \end{bmatrix}$$

$$\Delta = \begin{bmatrix} \Delta_1 & \Delta_{12} \\ \Delta_{21} & \Delta_2 \end{bmatrix} \tag{35}$$

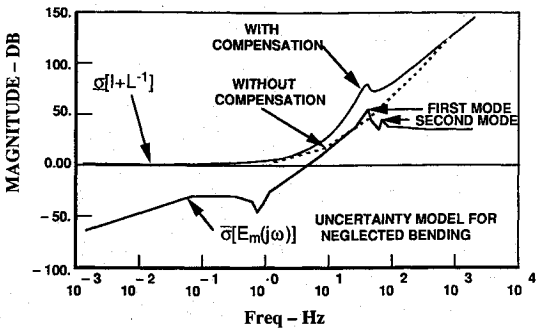

Fig. 7 Roll-yaw robustness to bending dynamics.

which shows output perturbations coupling into input channels (Δ_{12}) and input perturbations coupling into output channels (Δ_{21}). Our simultaneous input-output perturbation model, Fig. 3, requires that $\Delta_{12} = \Delta_{21} = 0$.

Both the PSPP and RS LQG/LTR roll-rate command autopilots were designed to have good input loop break point gain and phase margins. Figure 8 displays a matrix of the upper bound on the allowable perturbation, which varies the structure of the perturbations for these two designs. Columns 1 and 2 of Fig. 8 illustrate the perturbation structure, column 3 is the SSV μ-test applied to the PSPP design, and column 4 is the SSV μ-test applied to the RS LQG/LTR design. The upper bound on Δ is the multivariable stability margin.

Row 1 of Fig. 8 analyzes the unstructured input perturbation, with $\Delta = \Delta_1$ (2 × 2) a full matrix, and $\Delta_2 = 0$. In this case the SSV μ-test is equivalent to the stability robustness theorem 4. The upper bound on the allowable perturbation is taken as the $\min(\underline{\sigma}[I + L^{-1}(s)])$. For the PSPP design, it is 0.69 and for the RS LQG/LTR design, it is 0.74. The RS LQG/LTR design shows better robustness at the plant input. The PSPP design uses plant shaping gains [$K1$ through $K4$, Eq. (32)] to shape the zeros of the LTM, which decouples the aileron and rudder input channels.[17] The RS LQG/LTR design was shown to naturally decouple the roll and yaw loops through the penalty parameters in the linear quadratic regulator performance index design.[18] The larger upper bound on the allowable perturbation for the RS LQG/LTR design is attributed to the better input decoupling in that design.

Row 2 of Fig. 8 structures the input perturbation matrix $\Delta = \Delta_1$, which forces the matrix to be diagonal. This improves the PSPP perturbation upper bound. The RS LQG/LTR design did not appreciably change. By structuring Δ to be diagonal, we eliminate the cross-channel input perturbations. The large improvement in the PSPP upper bound again indicates that the PSPP controller does not input decouple as well as the RS LQG/LTR design.

Row 3 of Fig. 8 considers only output perturbations, with $\Delta = \Delta_2$ (3 × 3) a full matrix and $\Delta_1 = 0$. The stability robustness theorem 4 perturbation bound at the plant output is very small, which indicates almost no gain margin at the plant output. The LTM at the plant output is a 3 × 3 matrix, and at the plant input it is a 2 × 2 matrix. The units of the outputs are ft/s^2, rad/s, and rad/s. At the plant input, both control variables have units of radians. The mismatch of units at the plant output causes the conservative robustness prediction. Singular values are very sensitive to scaling. Scaling the acceleration output to have similar units (divide by velocity and convert acceleration to flight path angle rate) will improve the singular value computation.

The PSPP roll rate command autopilot, Eq. (32), does not use lateral acceleration. This allows us to reduce the open-loop plant model output vector to just roll rate p and yaw rate r. Thus, $G_0(s)$ and $K(s)$ become 2 × 2 square matrices, which creates a square system (controls equal outputs).We applied the SSV μ-test for $\Delta = \Delta_2$ a full 2 × 2 matrix, $\Delta_1 = 0$, and found that $\bar{\sigma}[\Delta] < 0.3106$. This is a much higher upper bound than in row 3, which indicates that the acceleration units did in fact cause the low output stability margin.

Row 4 of Fig. 8 also indicates this. By structuring the output perturbation matrix (making it diagonal), not allowing for cross-channel perturbations, the PSPP perturbation bound equals the input break point perturbation bound. We tested the square PSPP design with $\Delta = \Delta_2$ (2 × 2) diagonal and obtained the same result as row 4, 0.7107.

The RS LQG/LTR output break point perturbation bound, row 3, is also unrealistically small, i.e., 0.0137. In the RS LQG/LTR design, the Kalman filter processes lateral acceleration, roll rate p, and yaw rate r to estimate the state vector for feedback. We are not able to reduce the dimension of the plant model (number of outputs) since lateral acceleration is used. Thus, the poor scaling at the plant output is still a problem. By structuring the output perturbation matrix $\Delta = \Delta_2$ to be diagonal, row 4, the perturbation bound improves to 0.3591. This isolates the perturbation in the acceleration output channel from the other outputs. This eliminates the scaling problem in the singular value computation.

The remaining rows of Fig. 8 analyze the simultaneous input-output perturbations shown in Fig. 3. These results show that the perturbation upper bound depends upon the structure of the output perturbation matrix Δ_2 contained in Δ. The low output perturbation bounds shown in rows 3 and 4 are reflected in these results. As the matrix $\Delta = \text{diag}(\Delta_1, \Delta_2)$ becomes more structured, the perturbation bound improves.

Our results show the utility of the SSV μ-test in predicting multivariable stability margins. The small gain theorem, when used for this purpose, predicts very conservative stability margins. This demonstrates the conservatism when modeling the uncertainty as a full single-block matrix vs a multiple-block diagonal matrix.

Structured Uncertainty Analysis: Real Parameter Variations

In the previous section, the SSV μ-test was used to compute multivariable stability margins. The Δ matrix modeled complex variations introduced at the plant input and output loop break points. In this section the SSV μ-test is used to analyze real parameter variations (also denoted as Δ) modeled using a

UNCERTAINTY		PSPP	ROBUST SERVO
UNSTRUCTURED INPUT	Δ_1 - FULL MATRIX	$\bar{\sigma}[\Delta] < \underline{\sigma}[I+L^{-1}]$ $\bar{\sigma}[\Delta] < 0.6869$	$\bar{\sigma}[\Delta] < \underline{\sigma}[I+L^{-1}]$ $\bar{\sigma}[\Delta] < 0.7361$
STRUCTURED INPUT	$\Delta_1 = \begin{bmatrix} \delta_1 & 0 \\ 0 & \delta_2 \end{bmatrix}$	$\bar{\sigma}[\Delta] < 1/\mu$ $\bar{\sigma}[\Delta] < 0.7177$	$\bar{\sigma}[\Delta] < 1/\mu$ $\bar{\sigma}[\Delta] < 0.7362$
UNSTRUCTURED OUTPUT	Δ_2 - FULL MATRIX	$\bar{\sigma}[\Delta] < 1/\bar{\sigma}[M]$ $\bar{\sigma}[\Delta] < 0.0279$	$\bar{\sigma}[\Delta] < 1/\bar{\sigma}[M]$ $\bar{\sigma}[\Delta] < 0.0137$
STRUCTURED OUPUT	$\Delta_2 = \begin{bmatrix} \delta_1 & 0 & 0 \\ 0 & \delta_2 & 0 \\ 0 & 0 & \delta_3 \end{bmatrix}$	$\bar{\sigma}[\Delta] < 1/\mu$ $\bar{\sigma}[\Delta] < 0.7107$	$\bar{\sigma}[\Delta] < 1/\mu$ $\bar{\sigma}[\Delta] < 0.3591$
UNSTRUCTURED INPUT AND OUTPUT	Δ - FULL MATRIX	$\bar{\sigma}[\Delta] < 1/\bar{\sigma}[M]$ $\bar{\sigma}[\Delta] < 0.0031$	$\bar{\sigma}[\Delta] < 1/\bar{\sigma}[M]$ $\bar{\sigma}[\Delta] < 0.0031$
STRUCTURED INPUT AND OUTPUT	$\Delta = \begin{bmatrix} \Delta_1 & 0 \\ 0 & \Delta_2 \end{bmatrix}$	$\bar{\sigma}[\Delta] < 1/\mu$ $\bar{\sigma}[\Delta] < 0.0276$	$\bar{\sigma}[\Delta] < 1/\mu$ $\bar{\sigma}[\Delta] < 0.0136$
Δ_1 - FULL MATRIX Δ_2 - FULL MATRIX	$\Delta = \left[\begin{array}{cc:c} \delta_1 & 0 & 0 \\ 0 & \delta_2 & 0 \\ \hdashline 0 & 0 & \Delta_2 \end{array}\right]$	$\bar{\sigma}[\Delta] < 1/\mu$ $\bar{\sigma}[\Delta] < 0.0277$	$\bar{\sigma}[\Delta] < 1/\mu$ $\bar{\sigma}[\Delta] < 0.0136$
	$\Delta = \left[\begin{array}{c:cc} \Delta_1 & & \\ \hdashline & \delta_1 & \\ & & \delta_2 \delta_3 \end{array}\right]$	$\bar{\sigma}[\Delta] < 1/\mu$ $\bar{\sigma}[\Delta] < 0.4127$	$\bar{\sigma}[\Delta] < 1/\mu$ $\bar{\sigma}[\Delta] < 0.2976$
	$\Delta = \left[\begin{array}{c:cc} \delta_1 \delta_2 & & \\ \hdashline & \delta_1 & \\ & & \delta_2 \delta_3 \end{array}\right]$	$\bar{\sigma}[\Delta] < 1/\mu$ $\bar{\sigma}[\Delta] < 0.4185$	$\bar{\sigma}[\Delta] < 1/\mu$ $\bar{\sigma}[\Delta] < 0.3000$

Fig. 8 Perturbation bounds varying perturbation structure.

BDP structure (but with a different M matrix) as shown in Fig. 2b. The SSV μ produces conservative robustness bounds when analyzing problems containing real parameter variations. However, these conservative bounds still indicate the sensitivity to imperfect knowledge of design model coefficients. The flight condition analyzed in this section uses an unstable airframe model (trim angle of attack of 16 deg).

As in the case of complex variations, we must formulate the interconnection structure of Fig. 2b isolating the real parameters that are under perturbation. This section presents a method for formulating this structure and introduces the concept of perturbation rank. Note that the M matrix in Fig. 2b now models the effects of real parameter variations on the nominal closed-loop system and is different from the M matrix modeling complex variations at the plant input and output.

The BDP structure of Fig. 2b, with $\Delta = 0$, is a description of the nominal closed-loop system. The approach developed by Morton[10,11] creates a state space triple (A_m, B_m, C_m) for $M(s)$. Morton's technique isolates n real parameter variations into $\Delta = \text{diag}[\delta_i]$ by factoring out the variations in the closed-loop system matrix. Model the closed-loop system (using compensation) as

$$\dot{x} = A_{cl}x \tag{36}$$

The closed-loop system matrix A_{cl} is based upon uncertain parameters, and is modeled as

$$A_{cl} = A_0 + \sum_{i=1}^{n} E_i \delta_i \tag{37}$$

In Eq. (37) the matrices E_i are the structural definitions for each of the parameter perturbations δ_i. Using this model, each matrix E_i is decomposed using a SVD $E_i = U\Sigma V^*$. The matrix Σ will have k_i nonzero singular values where k_i is equal to the rank of the matrix E_i. The rank $(E_i) = k_i$ denotes the rank of the perturbation δ_i. The zero singular values of Σ are discarded, making Σ a $k_i \times k_i$ diagonal matrix. Using this new Σ,

$$E_i = \underbrace{U(\Sigma)^{1/2}}_{\beta_i} \underbrace{I_{ki}(\Sigma)^{1/2} V^*}_{\alpha_i} \tag{38}$$

$$E_i = \beta_i \alpha_i$$

where I_{ki} is an identity matrix of order k_i. The matrices β_i and α_i in Eq. (38) depend only upon the magnitude of the ith nominal parameter. The state space triple describing $M(s)$ is formed as

$$A_m = A_0; \qquad B_m = [\beta_1 \ldots \beta_n]; \qquad C_m = \begin{bmatrix} \alpha_1 \\ \vdots \\ \alpha_n \end{bmatrix} \tag{39}$$

If the state space description of the control system is linear in the uncertain parameters, Eq. (36), the Morton method is applicable. If the parameters multiply each other, then the method is no longer applicable.

Sensitivity to Uncertain Aerodynamic Stability Derivatives

The pitch flight control system model contains the following four uncertain aerodynamic parameters:

$$Z_\alpha = Z_{\alpha 0}(1 + \delta_1) \tag{40a}$$

$$Z_\delta = Z_{\delta 0}(1 + \delta_2) \tag{40b}$$

$$M_\alpha = M_{\alpha 0}(1 + \delta_3) \tag{40c}$$

$$M_\delta = M_{\delta 0}(1 + \delta_4) \tag{40d}$$

with each $|\delta_i| < 1$. When using the SSV μ, the above δ_i are treated as complex variations in the analysis; even though they are real. In some cases this may produce very conservative robustness bounds.

The closed-loop system matrix A_{cl} is then modeled as

$$A_{cl} = A_0 + E_1\delta_1 + E_2\delta_2 + E_3\delta_3 + E_4\delta_4 \tag{41}$$

with the δ_i defined in Eqs. (40).

An SVD of the matrices E_i, $i = 1, 2, 3, 4$ indicates that the uncertain aero parameters are all rank one perturbations. Using Eqs. (38) and (39) the triple A_m, B_m, C_m is computed. The software used here to compute μ vs frequency is the same as that used in the previous section (in the previous section the variation is complex, in this case it is real). Currently, there are several new approaches[19,20] available to compute μ for real parameter variations. However, reliable software is generally not available. We should note that the upper bound on the allowable perturbation computed using our software is conservative.

Weights γ_i on each parameter variation δ_i can be introduced where

$$\delta_i = \gamma_i \hat{\delta}_i \tag{42}$$

This yields

$$E_i = \beta_i \delta_i \alpha_i = \gamma_i \beta_i \hat{\delta}_i \alpha_i \tag{43}$$

where α_i and β_i are as defined as in Eq. (38).

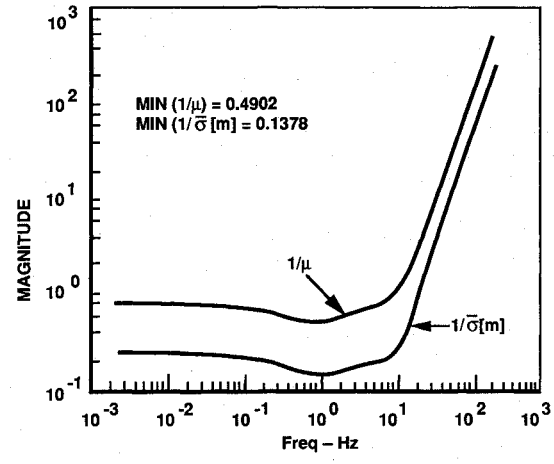

Fig. 9 Aerodynamic parameter SSV analysis.

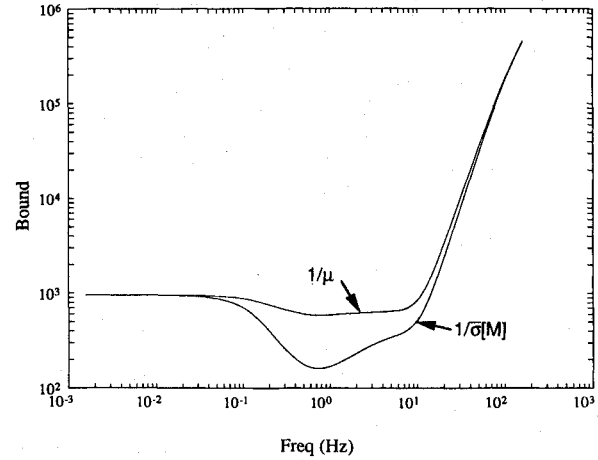

Fig. 10 Dynamic pressure SSV analysis.

Figure 9 displays the inverse of the SSV μ and $\bar{\sigma}[M]$ frequency response using unit weights ($\gamma_i = 1.0$). The infemum of $1/\mu$ and $1/\bar{\sigma}[M]$ from these curves are

$$\min(1/\mu) = 0.4902; \qquad \min(1/\bar{\alpha}[M]) = 0.1378 \qquad (44)$$

The SSV robustness test indicates a 49% allowable variation in the uncertain aerodynamic stability derivatives. If we apply the stability robustness theorem 4 (presented earlier), we obtain only a 14% variation bound. To determine the amount of conservatism present in this robustness bound, a Monte Carlo eigenanalysis was performed. Thousands of random closed-loop matrices were examined. The Monte Carlo prediction was 60–61%. At a 60% variation level, the closed-loop system was stable. At a 61% variation, several unstable closed-loop systems were formed. This missile autopilot application shows the SSV variation bound is in fact conservative.

In Wise[21] an exact bound on the aerodynamic stability derivatives was calculated using the De Gaston-Safonov[20] algorithm. The exact bound was computed at 60.44%. A software implementation of the De Gaston-Safonov[20] algorithm is presented in Wise.[22]

Variations in Dynamic Pressure Modeled as a Real Parameter Variation

Dynamic pressure Q (psf) is dependent upon air density ρ and missile velocity V through the relation $Q = 1/2\rho V^2$. The aerodynamic stability derivatives are linear functions of dynamic pressure. The aerodynamic stability derivative Z_α is obtained from

$$Z_\alpha = \frac{C_{z\alpha} QS}{mV} \qquad (45)$$

where $C_{z\alpha}$ is a nondimensional stability derivative, S is a reference area (ft^2), m is missile mass (lbm), and V is missile velocity. The other three aerodynamic stability derivatives are obtained in a similar fashion.

The SSV μ-test is applied to this problem using the closed-loop system model in Eq. (36). Let Q be modeled as $Q = Q_0 + \delta_1$. In this case Eq. (36) is $A_{cl} = A_0 + E_1\delta_1$. The matrix E_1 has rank equal to 2. The matrix Δ and M are

$$\Delta = \text{diag}(\delta_1\delta_1) \qquad (46)$$

$$M = C_m(sI - A_m)^{-1}B_m$$

Figure 10 displays the $1/\mu$ and $1/\bar{\sigma}[M]$ frequency responses. The minimums of these curves are $\min(1/\mu) = 583.8$, and $\min(1/\bar{\sigma}[M]) = 160.5$. The nominal value of Q is $Q_0 = 950.1$ (psf). The SSV robustness test predicts a 61.45% allowable variation. The small gain theorem predicts a 16.89% allowable variation. To determine how conservative these robustness predictions are, a root locus varying Q was computed and is shown in Fig. 11. Figure 11 is a plot of the eigenvalues of A_{cl} varying Q. The root locus plots show that the closed-loop system remains stable for a Q range of $95.0 < Q < 2Q_0$, which is slightly more than a 90% variation. This also demonstrates the conservatism in the SSV robustness prediction when evaluating robustness to real parameter variations.

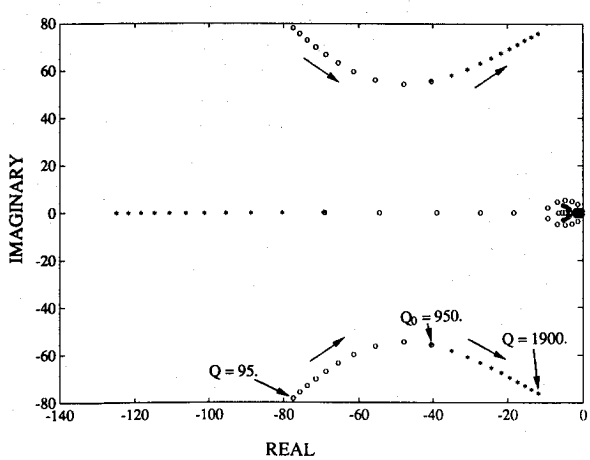

Fig. 11 Dynamic pressure root locus.

Conclusions

Robustness theorems by Doyle and Lehtomaki were used to determine autopilot sensitivity to neglected and mismodeled actuator dynamics and neglected bending dynamics. The actuator results determined the minimum actuator natural frequency required to guarantee stability. For our design example, this was 2.8 Hz. The bending analysis showed that bending compensation was required to remove flexible body effects in order to maintain closed-loop stability. It is evident that many of the classical loop-shaping concepts can be applied in shaping singular value frequency responses.

The structured singular value μ-test was found to be an excellent method for computing multivariable stability margins. These margins, based upon complex perturbations at the plant input and output, were found to be dependent upon the structure of the perturbation matrix Δ. The diagonal perturbation structures were found to yield the largest stability margins.

The block diagonal perturbation structure, used in the SSV analysis, was also applied to the problem of real parameter variations. The SVD of the perturbation structural definition matrices was easily automated. Application of the SSV μ-test yielded a 49.0% perturbation bound when all of the aeroparameters were allowed to vary. Although the SSV bound on real parameter variations is conservative, it still provides the design engineer with a computable measure of the sensitivity to imperfect knowledge of design model coefficients.

References

[1]"Multivariable Analysis and Design Techniques," AGARDograph Lecture Series 117, Oct. 1981.

[2]*IEEE Transactions on Automatic Control: Special Issue on Multivariable Control,* Vol. AC-26, No. 1, Feb. 1981.

[3]Anderson, B. D. O., and Moore, J. B., *Linear Optimal Control,* Prentice-Hall, Englewood Cliffs, NJ, 1971.

[4]Doyle, J. C., "Robustness of Multiloop Linear Feedback Systems," *Proceedings of the IEEE Conference on Decision and Control,* Inst. of Electrical and Electronics Engineers, Piscataway, NJ, 1978, pp. 12-18.

[5]Lehtomaki, N. A., "Practical Robustness Measures in Multivariable Control System Analysis," Ph.D. Dissertation, Massachusetts Inst. of Technology, Cambridge, MA, 1981.

[6]Safonov, M. G., "Stability Margins of Diagonally Perturbed Multivariable Feedback Systems," *Proceedings of the IEE,* Vol. 129, Pt. D, No. 6, 1982, pp. 251-256.

[7]Mukhopadhyay, V., and Newsom, J. R., "A Multiloop System Stability Margin Study Using Matrix Singular Values," *Journal of Guidance, Control, and Dynamics,* Vol. 8, No. 5, 1984, pp. 582-587.

[8]Doyle, J. C., "Structured Uncertainty in Control System Design," *Proceedings of the IEEE Conference on Decision and Control,* Inst. of Electrical and Electronics Engineers, Piscataway, NJ, 1985, pp. 260-265.

[9]Doyle, J. C., Wall, J. E., and Stein, G., "Performance and Robustness Analysis for Structured Uncertainty," *Proceedings of the 22nd IEEE Conference on Decision and Control,* Inst. of Electrical and Electronics Engineers, Piscataway, NJ, 1982, pp. 629-636.

[10]Morton, B. G., and McAfoos, R. M., "A Mu-Test for Robustness Analysis of a Real-Parameter Variation Problem," *Proceedings of the American Control Conference,* American Automatic Control Council, Boston, MA, 1985, pp. 135-138.

[11]Morton, B. G., "New Applications of Mu to Real Parameter Variation Problems," *Proceedings of the 24th IEEE Conference on Decision and Control,* Inst. of Electrical and Electronics Engineers, Piscataway, NJ, 1985, pp. 233-238.

[12]Kharitinov, V. L., "Asymptotic Stability of an Equilibrium Position of a Family of Systems of Linear Differential Equations," *Differentsial. Uravnen.,* Vol. 14, No. 11, 1978, pp. 2086-2088.

[13]Barmish, B. R., and DeMarco, C. L., "Criteria for Robust Stability With Structured Uncertainty: A Perspective," *Proceedings of the American Control Conference,* American Automatic Control Council, Boston, MA, 1987, pp. 476–481.

[14]Postlethwaite, I., and MacFarlane, A. G. J., *A Complex Variable Approach to the Analysis of Linear Multivariable Feedback Systems,* Springer-Verlag, New York, 1979.

[15]Athans, M., "Computer-Aided Control System Design," *Lecture Notes,* Massachusetts Inst. of Technology, Cambridge, MA, June 1986.

[16]Stewart, G. W., *Introduction to Matrix Computations,* Academic, New York, 1973.

[17]Wise, K. A., "Maximizing Performance and Stability Robustness in a Conventional Bank-to-Turn Missile Autopilot Design," AIAA Paper 88-C-1086, Dec. 1988.

[18]Wise, K. A., "Bank-to-Turn Missile Autopilot Design Using Loop Transfer Recovery," *Journal of Guidance, Control, and Dynamics,* Vol. 1, No. 1, 1990, pp. 145–152.

[19]Jones, R. D. "Structured Singular Value Analysis for Real Parameter Variations," *Proceedings of the AIAA Guidance, Navigation, and Control Conference,* AIAA, Washington, DC, 1987, pp. 1429–1432.

[20]De Gaston, R. R., and Safonov, M., "Exact Calculation of the Multiloop Stability Margin," *IEEE Transactions on Automatic Control,* Vol. 33, No. 2, 1988, pp. 156–171.

[21]Wise, K. A., "A Comparison of Six Robustness Tests Evaluating Missile Autopilot Robustness to Real Parameter Variations," *Proceedings of the American Control Conference,* American Automatic Control Council, Boston, MA, 1990, pp. 755–763.

[22]Wise, K. A., Mears, B. C., Tang, C.-K., and Godhwani, A., "A Convex Hull Program Evaluating Control System Robustness to Real Parameter Variations" *Proceedings of the AIAA Guidance, Navigation, and Control Conference,* AIAA, Washington, DC, 1990, pp. 223–231.